# Advances and Applications of Carbon-Metal Oxides Hybrids in Sensor Applications: a Review

**Vajiheh Alijani[1], Luigi Sangaletti[2], Lorenzo D'Arsiè[3], Andrea Goldoni[1]**

[1]Elettra Sincrotrone Trieste, s.s. 14 km 164.5 in Area Science Park, 34149 Trieste, Italy

[2] I-Lamp and Department of Mathematics and Physics, Università Cattolica del Sacro Cuore, via dei Musei 41, 25121, Brescia, Italy

[3]Department of Engineering, University of Cambridge, Cambridge CB3 0FA, United Kingdom

ABSTRACT

This review focuses on the recent developments of Carbon/metal Oxide hybrids for gas and biological sensing, which is one of the most important fields where these hybrids are efficiently applied. Carbon and metal oxides are excellent complementary materials: in hybrids, they compensate for the shortcomings of the single components and their combination creates new advantageous features. Intensive research has advanced the understanding of these materials, however, the complex array of possible carbon nanostructure shapes and different metal oxides present many unexplored areas. Current results are already exciting and promise even bigger improvements in sensing. We introduce the recent progress in this field and the key advantages of some nanostructures over each counterpart have been discussed and compared, presenting examples and emphasizing the most promising routes.

## 1. Introduction

Sensors are employed in many commercial applications such as household security, industrial emission control, biomedical, agricultural, and automotive [1]. Gas sensors made of metal-oxide (MO) semiconductors are highly attractive due to their high sensitivity, stability, low cost, and fast response. Many MOs are known to be suitable for detection of oxidizing, reducing, or combustible gases. The fundamental mechanism for gas detection in semiconductor gas sensors is controlled by the change in the surface electrical conductivity caused by the charge transfer/spillover of electrons during gas interaction with the surface[2]. In spite of the remarkable chemical stability and selectivity of MO based sensors, two major drawback of their application as gas sensing materials is their inherent high resistance and the room temperature low sensitivity. This is inconvenient for some practical applications and also makes them unsafe for detecting flammable gases like $H_2$. For example, $SnO_2$ sensors typically work between 200°-500º C with a detection limit in the range 30ppb to 500ppm depending on the detection gas.

In contrast with MO sensors, nanoscale carbon-based materials may combine excellent detection sensitivity with interesting transduction properties already at room temperature. Their conductivity is effectively altered by very small amounts of adsorbed gas molecules[3]. Generally, the electrical resistance of carbon nanostructures is modified by electron transfer between carbon nanostructures and oxidizing or reducing gas molecules adsorbed on their surface and this electrical charge transfer is found to be the major sensing mechanism[4]. For example when the p-type carbon nanotubes (CNTs) adsorb reducing molecules, their electrical resistance increases with the increase of the adsorbed gas molecules[5]. Currently carbon nanostructures such as CNTs, carbon nanofibers (CNFs), and carbon sponge attracted remarkable attention as potential candidates for sensors due to their large surface area, extraordinary conductivity, and high mechanical and thermal stability[6,7]. Beside these advantages, gas sensors based on carbon nanostructures exhibit certain limitations such as irreversibility, long recovery time and, particularly for pure pristine carbon materials like graphene and CNTs, lack of response toward many molecules and gases of interest[8,9,10] . The latter point can be overcome by engineering the nanoscale carbon materials, for example to create defects and graft functional groups to their surface in a controlled way.

In general, improvement in sensor applications should include enhanced gas sensitivity and selectivity, fast response and recovery time, as well as reduced operating temperature. These properties can be achieved by using carbon/MO hybrids, in order to develop systems with the high sensitivity toward the target molecules typical of MOs and the low or room temperature gas response available for nanostructured conductive carbons[1]. Moreover, the possibility to print the sensor on flexible substrates should not be underestimated. The resulting carbon/MO nanostructure hybrid materials not only combine these extraordinary properties, but also exhibit some new feature originated by the hybridization[11,12]. These composites are not merely the sum of the individual components, but rather new materials with new functionalities and properties. Some of the reported carbon/MO nanostructure hybrids exhibit higher sensitivity toward target gas at room temperature[8,13, 14] than the relative carbon sensors or MO sensors. The data reported so far suggest that the type of junctions that are generated at contact points and the formation of a p-n heterojunction between a typically p-type carbon support and a n-type MO may play a crucial role in the enhancement of the response[13]. From the viewpoint of structure the carbon support can induce the nucleation, growth and formation of fine metal oxide nano-/microstructures with uniform dispersion and controlled morphology, thereby avoiding the agglomeration of metal oxides. Reducing as much as possible the size of the MO clusters and avoiding their agglomeration is fundamental for the sensitivity and the response time, as shown in Fig. 1.

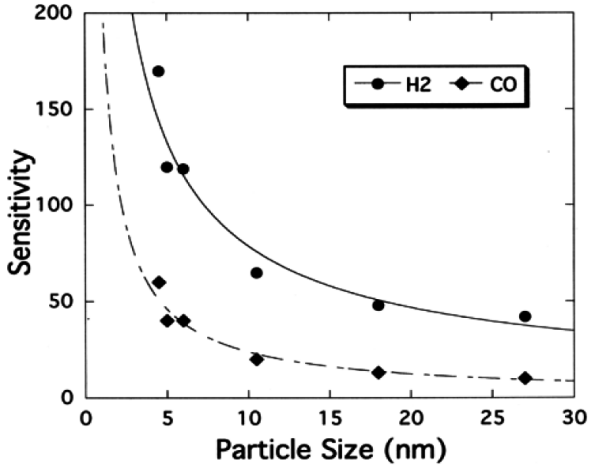


**Fig.1:** Sensitivity as a function of particle size for $H_2$ and CO.[13]

If the carbon component is a good electrical conductor, e.g., carbon nanofibers (CNFs), CNTs or graphene, the resulting composites can form a perfect integrated structure with a developed electron conductive network and shortened current transport paths, improving the poor electrical properties and charge transfer of pure metal oxides.

The used carbon nanostructures in carbon/MO nanostructure hybrids for application as sensors include mesopores carbon, SWCNTs, MWCNTs, CNFs, graphene, graphene oxide (GO), and reduced-GO. Significant synergistic effects, such as room-temperature sensing capability when exposed to low-concentration gases, such as $NO_2$, $H_2$, and CO, often occur in hybrid composites because of size effects and interfacial interactions in contrast to the high-temperature operation required for metal oxides alone.

## 2. Carbon-Metal Oxide Hybrids as Sensors

Recently, research is focusing on the fabrication of electrochemical sensors by combining the advantages of carbon nanostructures with other nano-structured materials like transition metals and MOs.

For example combination of some MOs include $MnO_2$[15], CuO[16], and NiO[17] and OMCs have been used to modify glassy carbon electrodes to improve the electroactivity and selectivity for glucose and $H_2O_2$. Among these carbon/MO nanocomposites, the carbon/$MnO_2$[15] nanocomposite modified glassy carbon electrode shows sensitivity to $H_2O_2$. Carbon/CuO[16] nanocomposite modified glassy carbon electrode and Carbon/NiO [61] [17] nanocomposite modified glassy carbon electrode are sensitive to glucose and can be used as biosensors to analyze glucose level in human blood serum samples. The Carbon/CuO[16] and carbon/NiO[17] hybrid glucose sensors exhibit a high sensitivity of 1154.1 $\mu Am^{-1} Cm^{-2}$ and 834.8 $\mu Am^{-1} Cm^{-2}$, respectively and also shows a low detection limit of 0.1 μM and 0.65 μM, respectively, at the signal to noise ratio of 3.

### 2.1 MO/CNTs

There are several reports on the enhanced gas and chemical sensing properties of MO/CNT hybrids, including fast response and recovery time and increased sensitivity. For example, Wei et al.[13] reported that a hybrid of (single-wall) SWCNTs/$SnO_2$ revealed

an enhanced sensitivity for $NO_2$. The authors concluded that a higher sensing behavior originated from a common interface with CNTs, since the morphology and surface area of the hybrid sensors were similar to those of the pure $SnO_2$ and the observed sensitivities increased with increasing CNT loading. Wisitsoraat et al.[18] reported that electron beam evaporation of a powder mixture of (multi-wall) MWCNTs and $SnO_2$ could enhance the ethanol sensing via an increase in the surface area of $SnO_2$. Espinosa et al.[19] reported that the pure $WO_3$ sensors, which are insensitive to $NO_2$ at low temperatures of operation, show sensitivity to this gas when hybridized with MWCNTs. Also Mao et al.[20] reported a hydrogen gas sensor using semiconducting SWCNT decorated with $SnO_2$ nanocrystals. This hybrid sensor showed a response time of 2–3 seconds to 1% $H_2$ under room temperature and can fully recover within a few minutes in air.

Up to now, various CNTs/MO hybrids have been examined for detection of various gases and chemicals. Investigated hybrid sensors based on MO and CNTs consist of MOs such as $SnO_2$[1,8,13,20–41], $WO_3$[42–45], $V_2O_4$[5,46], $In_2O_3$[47,48], ZnO[49–53], $Co_3O_4$[54–56], $TiO_2$[57–62], $Fe_2O_3$[63–65], CdO[66], CuO[67–72], $MnO_2$[73–75], $Cr_2O_3$[76], $ZrO_2$[77], $SiO_2$[78], $Cu_2O$[79,80], and NiO[80,81]. For example CNTs/$SnO_2$ based sensors have been examined for detection of some gases such as $NO_2$[1,13,24,31,32,34,36,39], $NH_3$[14,30,32,82], CO[23,31,38], $NO_x$[28], $H_2$[3,20,25,39, 80], $SO_2$[37], $H_2S$[41], and $O_3$[30,82] as well as detection of some chemicals such as ethanol[21,22,26,27,647,37,40,41], methanol[33,40,41], acetone[647,35], xylene[32], acetaldehyde[35] and formaldehyde[83]. Hybrid of $WO_3$ and CNTs showed sensitivity to the $NO_2$[42], CO[42], and $H_2$[43,44] gases. $ZrO_2$/CNT[77] and $Cr_2O_3$/CNT[76] nanocomposites showed high sensitivity and selectivity to the ethanol. ZnO/CNT hybrid has been tested for gases like $NO_2$[52], CO[49], $O_2$[52] and some chemicals like urea[53]. $Fe_2O_3$/CNT hybrid has been examined for $H_2S$[63] and $H_2O_2$[64,65]. The $Co_3O_4$/CNT composite showed a better response to the oxidizing gases such as $NO_x$[54], reducing gases such as $H_2$[54], CO[55] , and also to some chemicals like $H_2O_2$[56]. CNT hybrids containing CdO[66], CuO[69], and $MnO_2$[74] showed sensitivity to $H_2O_2$. $TiO_2$/CNT hybrids exhibited sensitivity to the NO[57], $H_2$[59], and $NH_3$[58,60,61] gases and $In_2O_3$/CNT hybrid showed sensitivity to the $NH_3$[47] and $NO_2$[48] gases. Furthermore $V_2O_4$/CNT hybrid showed sensitivity and selectivity to $NO_2$[5,46]. Also $Cu_2O$/[79], NiO/[81], $MnO_2$/[73], CuO/[67,68,70–72], and ZnO/[50,51] CNT based sensors have been used as biosensors for detection of glucose. Table

1 shows the comprehensive list of MO/C nanostructure hybrids, including MO/CNT hybrids, which have been fabricated and tested for gas-, chemical-, and bio- sensing.

Table 1. Comprehensive list of MO/C nanostructure hybrid sensors. The table is categorized by target molecules. The columns in this table show the MO in the hybrid sensor, the MO morphology, type of used carbon nanostructure, and related references, respectively. In this table CNT, SWCNT, MWCNT, *f*-CNT, CF, G, *f*-G, Gr, GO, rGO, C, CND, CNFL, MC, and OMC are referred to the carbon nanotube, single-walled carbon nanotube, multi-walled carbon nanotube, functionalized carbon nanotubes, carbon fiber, graphene, functionalized graphene, graphite, graphene oxide, reduced graphene oxide, carbon, carbon nano-dendrite, carbon nanoflakes, mesoporous carbon, and ordered mesoporous carbon, respectively.

| **Type of MO in the Hybrid Sensor** | **MO Morphology** | **Type of Carbon Nanostructure in the Hybrid sensor** | **Ref.** |
|---|---|---|---|
| **$NO_2$** | | | |
| $SnO_2$ | - | SWCNT | 13 |
| $SnO_2$ | Nanoparticle | CNT | 1,34 |
| $SnO_2$ | Nanoparticle | MWCNT | 32,36 |
| $SnO_2$ | Nanopowder | MWCNT | 24 |
| $SnO_2$ | Nanocluster | MWCNT | 31 |
| $SnO_2$ | Nanoparticle | SWCNT | 39 |
| $SnO_2$ | Nanoparticle | rGO | 1,85,86 |
| $SnO_2$ | Nanocrystals | rGO | 87 |
| $WO_3$ | Nanopowder | MWCNT | 19 |
| $WO_3$ | Film | MWCNT | 42,45 |
| $WO_3$ | Nanonudle | CF | 88 |
| $WO_3$ | Nanorod | C | 89 |
| $WO_3$ | Nanoparticle | G | 90 |
| $WO_3$ | Nanorod | G | 91 |
| $V_2O_4$ | Film | CNT | 5,46 |
| $V_2O_4$ | Film | CF | 92 |
| $Co_3O_4$ | Nanocrystal | rGO | 93 |

| | | | |
|---|---|---|---|
| $In_2O_3$ | - | CNT | 48 |
| ZnO | Nanoparticle | MWCNT | 52 |
| $Cu_2O$ | Nanowire | rGO | 94 |
| NiO | Nanosheet | rGO | 95 |
| **$NO_x$** | | | |
| $SnO_2$ | - | SWCNT | 28 |
| $Co_3O_4$ | Nanocrystal | SWCNT | 54 |
| $CeO_2$ | Nanoparticle | Gr | 96 |
| **NO** | | | |
| $TiO_2$ | Nanoparticle | SWCNT | 57 |
| **$NH_3$** | | | |
| $SnO_2$ | - | SWCNT | 30,82 |
| $SnO_2$ | Nanoparticle | MWCNT | 14,32 |
| $SnO_2$ | Nanoparticle | CNFL | 97 |
| $SnO_2$ | - | G | 98 |
| $MnO_2$ | - | GO | 99 |
| ZnO | Film | MWCNT | 100 |
| ZnO | Nanorod | CND | 101 |
| $In_2O_3$ | Nanotube | CNT | 47 |
| InSnO | Nanoparticle | SWCNT | 102 |
| $TiO_2$ | Nanoparticle | MWCNT | 61 |
| $TiO_2$ | Film | MWCNT | 58,60 |
| **CO** | | | |
| $SnO_2$ | Nanoparticle | SWCNT | 38 |
| $SnO_2$ | Nanocluster | MWCNT | 31 |
| $SnO_2$ | Nanopowder | MWCNT | 24 |
| $SnO_2$ | - | MWCNT | 23 |
| $WO_3$ | Nanopowder | MWCNT | 24 |
| ZnO | Nanoparticle | MWCNT | 49 |

| | | | |
|---|---|---|---|
| $Co_3O_4$ | Nanoparticle | *f*-CNT | 55 |
| **$CO_2$** | | | |
| $Sb_2O_3$ | Quantum dots | G | 103 |
| $SiO_2$ | Nanoparticle | CNT | 78 |
| **$H_2$** | | | |
| $SnO_2$ | Nanoparticle | SWCNT | 8 |
| $SnO_2$ | Nanoparticle | SWCNT | 39 |
| $SnO_2$ | - | SWCNT | 25 |
| $SnO_2$ | Nanocrystal | SWCNT | 20 |
| $SnO_2$ | Nanoparticle | rGO | 104 |
| $WO_3$ | Nanoparticle | MWCNT | 43 |
| $WO_3$ | Film | MWCNT | 44 |
| ZnO | Nanoparticle | G | 105 |
| $Co_3O_4$ | Nanocrystal | SWCNT | 54 |
| $MnO_x$ | Nanoparticle | MWCNT | 75 |
| $TiO_2$ | Nanoparticle | CNT | 59 |
| $Cu_2O$ | Nanoparticle | MWCNT | 80 |
| NiO | Nanoparticle | MWCNT | 80 |
| **$SO_2$** | | | |
| $SnO_2$ | Nanoparticle | MWCNT | 37 |
| **$H_2S$** | | | |
| $SnO_2$ | Nanoparticle | CNT | 41 |
| $SnO_2$ | Nanorod | G | 85 |
| $SnO_2$ | Nanocrystals | rGO | 106 |
| $Cu_2O$ | Nanocrystal | *f*-G | 107 |
| $Fe_2O_3$ | Nanotube | CNT | 63 |
| **$H_2O_2$** | | | |
| CdO | Nanoparticle | MWCNT | 66 |
| $Co_3O_4$ | Nanoparticle | MWCNT | 56 |

| | | | |
|---|---|---|---|
| $Co_3O_4$ | Nanoparticle | G | 108 |
| CuO | Nanoflower | MWCNT | 69 |
| CuO | Nanoparticle | rGO | 109 |
| $Cu_2O$ | Nanocubes | G | 110 |
| $Fe_2O_3$ | Nanoparticle | MWCNT | 64 |
| $Fe_2O_3$ | Nanoparticle | MWCNT | 65 |
| $Fe_3O_4$ | Nanoparticle | G | 111 |
| $Fe_3O_4$ | Nanoparticle | rGO | 112 |
| $MnO_2$ | Nanoparticle | MWCNT | 74 |
| $MnO_2$ | Nanoparticle | GO | 113 |
| $MnO_2$ | - | G/CNT | 114 |
| $MnO_2$ | Nanoparticle | OMC | 15 |
| $Mn_3O_4$ | - | 3D G foam | 115 |
| ZnO | - | rGO | 116 |
| $CeO_2$ | Nanoparticle | rGO Xerogel | 117 |
| **$O_2$** | | | |
| ZnO | Nanoparticle | MWCNT | 52 |
| ZnO | Nanowire | G | 118 |
| $TiO_2$ | Film | G | 119 |
| **$O_3$** | | | |
| $SnO_2$ | - | SWCNT | 30,82 |
| **Ethanol** | | | |
| $SnO_2$ | Film | MWCNT | 18 |
| $SnO_2$ | Nanotube | CNT | 29 |
| $SnO_2$ | Nanoparticle | CNT | 41 |
| $SnO_2$ | - | MWCNT | 27,37 |
| $SnO_2$ | Nanoparticle | MWCNT | 21,22 |
| $SnO_2$ | Mesoporous Nanoparticle | C | 120 |
| $SnO_2$ | Nanocrystals | rGO | 106 |

| | | | |
|---|---|---|---|
| $SnO_2/TiO_2$ | - | CNT | 26 |
| $Cr_2O_3$ | Nanotube | MWCNT | 76 |
| $ZrO_2$ | Nanoparticle | CNT | 77 |
| $Al_2O_3$ | Nanoparticle | G | 121 |
| $Fe_2O_3$ | Nanoparticle | G | 122 |
| ZnO | Nanoparticle | C | 123 |
| ZnO | Nanorod | rGO | 124 |
| **Methanol** | | | |
| $SnO_2$ | Nanoparticle | CNT | 41 |
| $SnO_2$ | Film | CNT | 33 |
| $Co_3O_4$ | Nanocrystal | rGO | 93 |
| NiO | Nanoparticle | G | 125 |
| $Fe_2O_3$ | - | C | 126 |
| **Acetone** | | | |
| $SnO_2$ | Nanoparticle | CNT | 29 |
| $SnO_2$ | Nanoparticle | MWCNT | 35 |
| $Fe_2O_3$ | - | C | 126 |
| $ZnFe_2O_4$ | Nanoparticle | G | 127 |
| ZnO | Nanoparticle | C | 123 |
| **Xylene** | | | |
| $SnO_2$ | Nanoparticle | MWCNT | 32 |
| **Acetaldehyde** | | | |
| $SnO_2$ | Nanoparticle | MWCNT | 35 |
| **Formaldehyde** | | | |
| ZnO | Quantum dots | G | 83 |
| **Urea** | | | |
| ZnO | - | MWCNT | 53 |
| **Glucose** | | | |

| | | | |
|---|---|---|---|
| $Cu_2O$ | Nanospindle | MWCNT | 79 |
| $Cu_2O$ | Nanocube | G | 110 |
| $Cu_2O$ | Nanosphere | rGO | 127 |
| $Cu_2O/NiO_x$ | Nanoparticle | GO | 129 |
| CuO | - | SWCNT | 71 |
| CuO | Nanoparticle | MWCNT | 68,70,72 |
| CuO | Nanoleaves | MWCNT | 70 |
| CuO | Nanoparticle | G | 130–132 |
| CuO | Nanocube | G | 133 |
| CuO | Nanoparticle | GO | 134 |
| CuO | Nanoneedle | G/CF | 135 |
| CuO | Nanoparticle | MC | 16 |
| CuO | Nanoparticle | CF | 136 |
| NiO | Nanoparticle | SWCNT | 81 |
| NiO | Nanofiber | GO | 137 |
| NiO | Nanoparticle | GO | 138 |
| NiO | Nanoparticle | G | 125,139 |
| NiO | Nanoparticle | OMC | 17 |
| NiO | Nanoparticle | C | 140 |
| $MnO_2$ | - | MWCNT | 73 |
| ZnO | Nanoparticle | SWCNT | 51 |
| ZnO | - | MWCNT | 50 |
| ZnO | Nanoparticle | rGO | 141 |
| ZnO | Nanoparticle | G | 142 |
| $TiO_2$ | Nanocluster | rGO | 143 |
| $Co_3O_4$ | Nanoparticle | G | 108 |
| $Co_3O_4$ | Nanowires | 3D G foam | 175 |
| $Mn_3O_4$ | - | 3D G foam | 115 |

In all examples of MO/CNT hybrids for sensor application, the improved sensing performance of hybrids in detecting both oxidizing (such as $NO_2$) and reducing (such as $H_2$, $NH_3$, and ethanol) agents is contributed to the synergistic effect of MOs and CNTs. In addition, the p−n heterojunction formed between, e.g., an n-type metal oxide and a p-type carbon support plays an important role in the sensing mechanism of MOs coated carbon heterostructures.

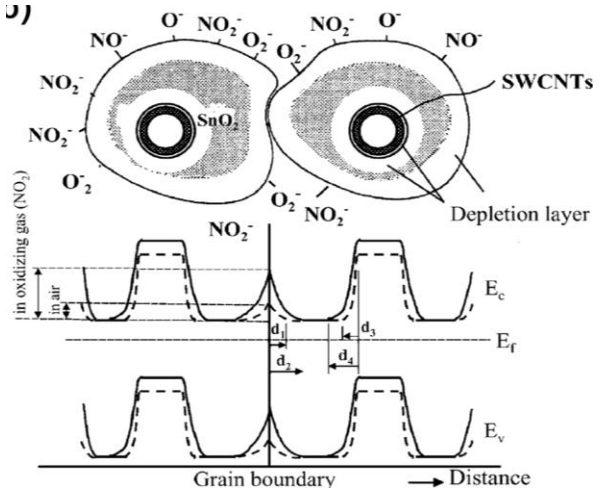


**Fig.2.** Potential barriers to electronic conduction at grain boundary for SWCNTs/$SnO_2$ sensors. $d_1$, $d_3$, $d_2$, and $d_4$ are the widths of depletion layers on the surface of the $SnO_2$ before adsorption of $NO_2$, in the interface between SWCNTs and $SnO_2$ before adsorption of $NO_2$, on the surface of the $SnO_2$ after adsorption of $NO_2$, and in the interface between SWCNTs and $SnO_2$ after adsorption of $NO_2$, respectively.[13]

In these hybrids the main role of MOs is detection of target molecule and it considered as sensing layer while the carbon support provides mainly the higher surface area and electronic conduction path. Although the mechanism of gas sensing in these hybrids is still poorly understood, the data reported so far suggest a mechanism of response based on the development of two depletion layers[13], one at the surface of MO grains and another at the interface of the n-type MO and p-type carbon support. Wei et al.[13] have studied the $SnO_2$/SWCNTs hybrids as $NO_2$ sensors and presented a model to relate potential barriers to electronic conduction in the hybrid materials. This model suggests

that the high sensitivity in the hybrids is associated with the stretching of these depletion layers when detected gases are adsorbed. For example in the case of $SnO_2$/CNT hybrid[13] when the target gas is $NO_2$, the first depletion layer creates by absorbing $NO_2$ gas molecules on the surface of $SnO_2$. The adsorbed $NO_2$ gas molecules extract electrons from the MO and leave the oxide surface positively charged. This leads to the formation of a depletion zone on the surface of the MO and to an increase in the sensor resistance. At the same time, $NO_2$ interacts with the p-n heterojunctions (junction between n-type MO and p-type carbon support) and causes the formation of additional depletion layer. In this case the possible changes in potential barriers inside the $SnO_2$ layer or at the interfaces between $SnO_2$ and the layer of p-SWCNTs expand the depletion layers at the p-n junctions of the $SnO_2$ substrate, which then amplifies the increase in the resistance upon $NO_2$ adsorption and enables the operation of the gas sensor at room temperature. Fig. 2 shows presence of depletion zones near the CNT/MO interface. It is notable to mention that the barrier height between CNTs and $SnO_2$ grains vary for different gases[2]. For example exposure of $SnO_2$/CNT hybrid to the reducing gases such as ethanol[22], $NH_3$[14], or acetylene[84] has been shown to release electrons and consequently reduce the sensor resistance (in contrast with $NO_2$).

This picture was later considered by Marichy *et al.*[144] that have systematically investigated the role of CNT-CNT, CNT-MOs, and CNT-MOs-MOs-CNT junctions on the overall sensor performances. The capability to tune the type and number of junctions was achieved by conformally coating CNTs with $SnO_2$ layers deposited by ALD. In order to rationalize their behavior, the heterostructures were regarded as a field effect transistor, where the source is the contact between two $SnO_2$ layers, as well as the surface of the metal oxide, and the drain is constituted by the CNTs in contact with themselves and the device electrodes. The CNT−$SnO_2$ heterojunction corresponds to the gate and the space charge region of the depletion layer is modulated by the adsorption of the target gas on the MOs surface. In this perspective, the MOs−CNT interface can be regarded as a conductivity channel, which can be more or less opened or pinched, resulting in the amplification of the signal determined by the presence of adsorbed target gas species. In the same study, a similar explanation was suggested also for the $SnO_2$@reduced-GO composites, where two depletion layers were found to coexist, one

at the surface of the MOs particles and the one at the MOs-RGO interface. In this case the adsorbed gas species are supposed to modulate both depletion layers.

In view of device engineering, a fine-tuning of the sensing characteristics could therefore be achieved by controlling (i) the surface density of the MO nanoparticles onto the nanostructured carbon support or (ii) the thickness of the active layer, e.g. by the number of metal oxide ALD cycles. It is worth observing that when the metal oxide shell presents a thickness smaller or equal to its Debye length, its surface can be fully depleted by the gas adsorption, which in turn can strongly modify the heterojunction layer as in Ref.[145] where it was shown that the $SnO_2$ layer with thickness in the range of $SnO_2$ Debye length presented the highest sensing response, due to the full depletion of the oxide film.

The role of junctions was also postulated by Llobet *et al.*[146] to rationalize the improved performances of hybrid oxide-CNT layers, where the tested oxides were $WO_3$, $TiO_2$,and $SnO_2$. Also in this case, a mechanism of the gas response based on the development of two depletion layers, one at the surface of the metal oxide grain and another at the interface of the n-metal oxide/p-MWCNT heterostructure was considered.

The studies so far mentioned indicate that the model for gas-sensing layer interaction can significantly depend on the morphology of the layer at the nanoscale. Indeed, the MO can wrap the tube, virtually leaving no space for a direct absorption of the gas molecule on the CNT. Alternatively, when the MO nanoparticles are distributed on the CNT (or CNT bundle) layer without completely covering the CNTs, both a direct interaction with the CNTs and a nanoparticle-mediated interaction can occur.

It is worth noting that the picture so far drawn on the mechanisms at the basis of the CNT-MOs interaction with target molecules can be shared with all-oxide systems where nearly 2D oxide nanostructured were matched with MO nanoparticles. Liu *at al.*[147] considered vanadium oxide nanobelts coated with MOS nanoparticles such as $Fe_2O_3$, $TiO_2$ and $SnO_2$ to be employed as hybrid sensor nanostructures for sensing ethanol vapours. The enhanced sensitivity with respect to the bare $V_2O_5$ system was ascribed to the synergy between electrical transport through the largely depleted nanobelts and the

effective gas sensing on the high surface area MOS nanoparticles that can inject electrons into the nanobelts. Likewise, Woo *et al.*[148] considered ZnO nanowires coated with $Cr_2O_3$ oxide nanoparticles for the detection of trimetilammine (TMA). The highly selective and sensitive detection of TMA that was achieved by the deposition of semielliptical $Cr_2O_3$ nanoparticles on ZnO NW networks was explained by the catalytic effect of $Cr_2O_3$ and the extension of the electron depletion layer via the formation of p–n junctions.

Furthermore, the effects of oxygen adsorbed on the MO-CNT sensing layer should also be accounted for. This was discussed by Lu *et al.*[149] that considered discrete $SnO_2$ nanocrystals supported on an individual CNT used as a new gas-sensing platform. According to this study, the sensing performance of the hybrid nanostructure sensor could be related to the effective electron transfer between $SnO_2$ nanocrystals and MWCNTs and to the increase in the specific surface area of hybrid nanostructures. In open air, formation of oxygen adsorbates on the surface of $SnO_2$ and CNTs results in an electron-depleted surface layer due to electron transfer from the $SnO_2$–CNTs to oxygen. On this basis, two possible sensing mechanisms could be expected. The first involve target gas molecules (e.g., $NO_2$) that directly adsorb onto the $SnO_2$–CNT surface similarly to $O_2$ inducing an electron transfer and a change of the electrical conductivity. The second is related to the catalytic reaction of the target gas with oxygen adsorbates releasing electrons back to the $SnO_2$–CNT surface and changing electrical conductivity.

The role of the MO nanoparticle as catalyst was also invoked by Jung *et al.*[150] to discuss the increased sensitivity to humidity displayed by an $MnO_2$ coated CNT yarn. Here an increase in humidity causes a decrease in the hole density of p-type nanotubes, which in turn results in an increase in the resistance of the sensors. The $MnO_2$-coated sensor showed better sensitivity than the uncoated sensor as the Active $MnO_2$ material serves as a catalyst for promoting charge transfer between the $H_2O$ molecules and the CNTs by forming a p–n heterojunction .

In the discussion on catalytic effects the issue of photocatalysis deserves particular attention, as it involves titaniun dioxide, one of the most used MO material[151]. For

example the enhanced sensitivity to NO displayed by the anatase $TiO_2$ – CNT hybrid system was explained invoking the photocatalytic role of $TiO_2$ under UV light irradiation[152]. UV light (□=377 nm) was used to irradiate SWCNT-$TiO_2$ hybrids during the absorption of NO target molecules. When anatase $TiO_2$ is activated by UV light, electrons are generated from $TiO_2$ and transferred to SWCNT. This may result in an efficient transfer of electrons from SWCNT to the NO molecule and determine (i) a rapid recovery to the initial state and (ii) higher sensitivity of the active layer to the target gas.

Finally, the higher sensitivity to ammonia registered in ITO-CNT hybrid system with respect to the bare CNT bundle layer was explained by Rigoni *et al.* [102,153] by considering possible compensation effects established at the junction between the n-type oxide and the p-type CNTs. Compensation effects have been evidenced and discussed in Ref.[154], where CNTs exposed to water showed a crossover from p-type behavior to n-type behavior with water concentration increase. The crossover was ascribed to the reducing behavior of water, that at high concentrations could inject so many electrons into the CNTs to bring the Fermi level from the valence band of a semiconducting p-type system (Fig. 3, [155]), above the gap and then into the otherwise unoccupied conduction band.

In this frame the n-type oxide can reduce the p-type character of the CNT bundles that are found to display an increased resistivity once the junctions are formed. This resistivity increase is related to an upward shift of the Fermi level, which may ultimately turn the p-type CNT into an n-type layer when the system interacts with reducing molecules such as ammonia and water.

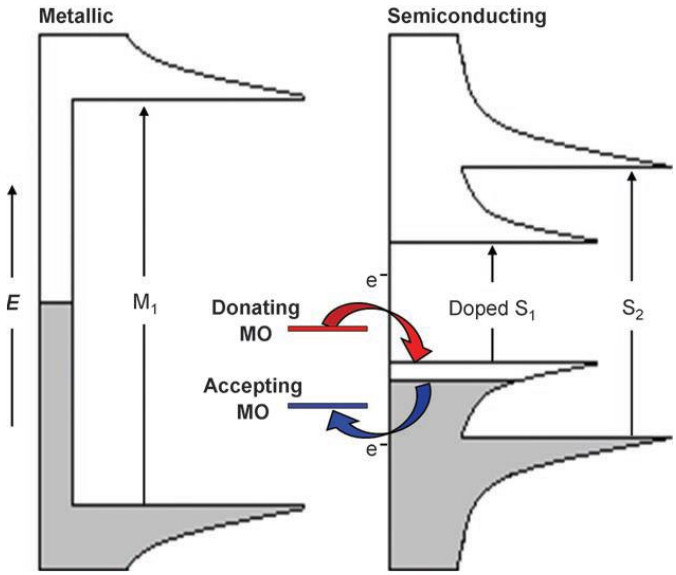


**Fig. 3**. Density-of-states diagram representing the relative energy matching of the SWNT valence (S1) band with interacting molecular orbitals (MOs) in two different scenarios: 1) interaction with an electron- donating MO and 2) interaction with an electron-accepting MO. In order for a MO to donate electronic density it must reside at a higher energy than the p-doped SWNT valence band; accordingly to accept electronic density it must be partially vacant and reside slightly lower in energy with respect to SWNT valence band. [155]

### 2.2 MO/Carbon Nanofiber

Another type of 1D carbon nanostructures, CNFs, have been used as gas sensors in the form of hybrids with MOs. CNF hybrids containing $V_2O_4$[92] and $WO_3$[88] have been tested for the sensor toward $NO_2$. The $NO_2$ sensor made with the hybrid of CNFs and $WO_3$ nanonodules showed sensing performance comparable to those made with conventional MO-based nanomaterials and pristine CNTs[88]. Also CuO/CNF hybrids have been fabricated and tested for glucose detection[136]. In a recent study, the designed sensor with CuONPs/CNFs nanocomposite modified glassy carbon electrode exhibited a wide linear response to glucose ranging from $5.0 \times 10^{-7}$ to $1.1 \times 10^{-2}$ M with a low detection limit down to 0.2 μM at the signal to noise ratio of 3 and a high sensitivity of 2739 μA $mM^{-1}$ $cm^{-2}$. According to the performance comparison of this sensor with other cupric oxide-based nonenzymatic sensors such as CuONPs/MCs[16], CuONPs/graphene[132], and CuONPs/MWCNTs[67,68], CuONPs/CNFs[136] electrode exhibits a higher sensitivity and wider linear range. This good performance could be attributed to the combined enhancement effect of CuONPs and CNFs.

### 2.3 MO/ Graphene, graphene oxide and foam

The rapid development of graphene provides new opportunities for the progress of analytical sensing systems with exceptional low noise to signal ratios for the detection of various chemical species and gases. More than graphene, graphene functionalized by oxygen containing species such as O, -OH and -OOH groups (known as rGO) at defective surfaces or edges of the pristine nanosheets has also been reported as a useful material for developing gas sensors[93,156]. In comparison with graphene, rGO showed desirable features such as ultra-low noise and ultra-low detection limit[93]. Robinson et al.[157] demonstrated reduced graphene oxide as the active material for high-sensitive gas sensors. Although graphene and rGO present excellent sensitivities to gas molecules, the performance of the sensors should be further improved to meet the requirements of practical gas sensors (such as having a low detection limit and high selectivity)[87]. To fulfill these requirements, one effective strategy is blending them with MO

nanostructures to form hybrid architectures, which could improve the sensor performance in terms of sensitivity, detection limit, response time, or recovery time[87].

To date, a large number of research publications based on graphene-, graphene oxide-, and reduced graphene oxide- MO hybrids for application in gas sensors have been reported. Hybrid sensors involve the MOs like $SnO_2$[1,85–87,98,104,106,158], $WO_3$[90,91], ZnO[83,100,105,116,118,124,141,142], $Co_3O_4$[93,108], $TiO_2$[119,143], $Fe_2O_3$[739], $Fe_3O_4$[111,729], CuO[109,130–135], $MnO_2$[99,113,114], $Cu_2O$[94,107,110,127,129], NiO[95,125,129,137–139], $Al_2O_3$[121], $Sb_2O_3$[103], and $ZnFe_2O_4$[127]. These types of hybrids show sensitivity to some gases and chemicals like $NO_2$, $NH_3$, methanol, ethanol, $H_2$, $H_2O_2$, $H_2S$, $O_2$, $CO_2$, formaldehyde, acetone, and glucose. For example the response of $WO_3$ nanorods/3.5 wt% graphene nanocomposites to $NO_2$ was up to 25 times higher than that of pure $WO_3$ nanorods[91]. The $SnO_2$/rGO nanostructures showed enhanced sensing performance compared with the corresponding pure systems as a consequence of synergistic effects between the different components in the composites[104]. Also the synergistic interface effect in $Cu_2O$ mesocrystal/rGO hybrid material makes that the response to 2 ppm $NO_2$ was 67.8%, much higher than that of rGO (22.5%) or $Cu_2O$ nanowires (44.5%) alone[94]. In the other hand incorporation of nanoparticles into graphene sheets prevents graphene from becoming agglomerated and also helps in achieving a good distribution of nanoparticles. Thus, the effective surface area available for the gas interaction increases by several times.

Among different types of 3D graphene structures, graphene foam[175,115] and graphene xerogel[117] were fabricated in the form of hybrid with MOs for application as sensors. The three dimensional architecture of graphene foam provides a large surface area for the construction of graphene- based nanocomposites without agglomeration. In addition, owing to its mechanical strength and flexibility, 3D graphene foam can be used as a freestanding electrode, where charge carriers could move along the continuous graphene skeleton with a small resistance. Recently two composite material based on 3D graphene foam and MOs include $Co_3O_4$/3DGF[175] and $Mn_3O_4$/3DGF[115] were fabricated and their sensing performance through glucose and $H_2O_2$ have been investigated. $Co_3O_4$/3DGF[175] show high sensitivity for nonenzymatic biosensing of glucose but offers a relatively small linear response range (up to 80 mM) due to the thick coating layer of $Co_3O_4$. This hybrid can detect glucose with an ultrahigh sensitivity of 3.39 mA $mM^{-1}$ $cm^{-2}$ and a remarkable

lower detection limit of <25 nM (S/N = 8.5) but could not be used for the detection of $H_2O_2$. In the other hand, composite of $Mn_3O_4$/3DGF[115] can be used as a highly sensitive and enzymeless sensor for detection of both glucose and $H_2O_2$. $Mn_3O_4$/3DGF- based glucose sensor achieved a large linear detection range of 0.1–8 mM, which is 2 orders of magnitude larger than that of $Co_3O_4$/3DGF. The authors contribute this large linear detection range to the excellent electrocatalytic activity of nanostructured $Mn_3O_4$, good conductivity of graphene, great abundance of catalytic sites and high specific surface area of the composite material.

## 3. Conclusions

Development of gas sensors using hybrid carbon/MO materials, typically carbon-based substrates decorated by metal oxide nanoparticles, is a new research area attracting recently much interest. By selection of appropriate oxides, high sensitivity and selectivity, at low power consumption may be achieved in gas sensing using CNT based devices, with possible applications in different technological processes for gas sensing even at a room temperature. This is a great advantage over conventional gas sensors based on metal oxide thin films like $SnO_2$, which are known to be efficient only at temperatures as high as 200-300 °C.

## Acknowledgments

This work is partly supported by the Italian MIUR projects FIRB "Nanosolar" RBAP11C58Y for V.A. and A.G. and by the European Community through the ENIAC Joint Undertaking–ERG (Grant Agreement No. 270722-1-ERG) for A.G.

LS acknowledges support from the UNICATT D.3.2 project ANAPNOI (2016-2018).

## References


1. C. Marichy, P. A. Russo, M. Latino, J.-P. Tessonnier, M.-G. Willinger, N. Donato, G. Neri and N. Pinna, *J. Phys. Chem. C*, 2013, **117**, 19729.
2. D. Eder, *Chem. Rev.*, 2010, **110**, 1348–85.
3. J. Kong, N. R. Franklin, C. Zhou, M. G. Chapline, S. Peng, K. Cho and H. Dai, *Science*, 2000, **287**, 3–625.
4. J. Kong, M. G. Chapline and H. Dai, *Adv. Mater.*, 2001, **13**, 1384–1386.
5. M.-G. Willinger, G. Neri, E. Rauwel, A. Bonavita, G. Micali and N. Pinna, *Nano Lett.*, 2008, **8**, 4201–4.
6. E. Llobet, *Sensors Actuators B Chem.*, 2013, **179**, 32–45.
7. W. Yuan and G. Shi, *J. Mater. Chem. A*, 2013, **1**, 10078.
8. M. Yang, D.-H. Kim, W.-S. Kim, T. J. Kang, B. Y. Lee, S. Hong, Y. H. Kim and S.-H. Hong, *Nanotechnology*, 2010, **21**, 215501.
9. R. Larciprete, L. Petaccia, S. Lizzit and A. Goldoni, *J. Phys. Chem. C*, 2007, **111**, 12169–12174.
10. A. Goldoni, L. Petaccia, S. Lizzit and R. Larciprete, *J. Phys. Condens. Matter*, 2010, **22**, 013001.
11. Y. Zhao, J. Li, C. Wu and L. Guan, *Nanoscale Res. Lett.*, 2011, **6**, 71.
12. H. Chu, L. Wei, R. Cui, J. Wang and Y. Li, *Coord. Chem. Rev.*, 2010, **254**, 1117–1134.
13. B.-Y. Wei, M.-C. Hsu, P.-G. Su, H.-M. Lin, R.-J. Wu and H.-J. Lai, *Sensors Actuators B Chem.*, 2004, **101**, 81–89.
14. N. Van Hieu, L. T. B. Thuy and N. D. Chien, *Sensors Actuators B Chem.*, 2008, **129**, 888–895.
15. L. Luo, F. Li, L. Zhu, Z. Zhang, Y. Ding and D. Deng, *Electrochim. Acta*, 2012, **77**, 179–183.
16. J. Zhang, N. Ding, J. Cao, W. Wang and Z. Chen, *Sensors Actuators B Chem.*, 2013, **178**, 125–131.
17. L. Luo, F. Li, L. Zhu, Y. Ding, Z. Zhang, D. Deng and B. Lu, *Colloids Surf. B. Biointerfaces*, 2013, **102**, 307–11.

18. A. Wisitsoraat, A. Tuantranont, C. Thanachayanont, V. Patthanasettakul and P. Singjai, *J. Electroceramics*, 2006, **17**, 45–49.
19. E. H. Espinosa, R. Ionescu, E. Llobet, A. Felten, C. Bittencourt, E. Sotter, Z. Topalian, P. Heszler, C. G. Granqvist, J. J. Pireaux and X. Correig, *J. Electrochem. Soc.*, 2007, **154**, J141.
20. S. Mao, S. Cui, K. Yu, Z. Wen, G. Lu and J. Chen, *Nanoscale*, 2012, **4**, 1275–9.
21. Y.-L. Liu, H.-F. Yang, Y. Yang, Z.-M. Liu, G.-L. Shen and R.-Q. Yu, *Thin Solid Films*, 2006, **497**, 355–360.
22. Y. Chen, C. Zhu and T. Wang, *Nanotechnology*, 2006, **17**, 3012–3017.
23. A. Yang, X. Tao, R. Wang, S. Lee and C. Surya, *Appl. Phys. Lett.*, 2007, **91**, 133110.
24. E. Espinosa, R. Ionescu, B. Chambon, G. Bedis, E. Sotter, C. Bittencourt, A. Felten, J. Pireaux, X. Correig and E. Llobet, *Sensors Actuators B Chem.*, 2007, **127**, 137–142.
25. J. Gong, J. Sun and Q. Chen, *Sensors Actuators B Chem.*, 2008, **130**, 829–835.
26. N. Van Duy, N. Van Hieu, P. T. Huy, N. D. Chien, M. Thamilselvan and J. Yi, *Phys. E*, 2008, **41**, 258–263.
27. O. A. Sahraei, A. Khodadadi, Y. Mortazavi, M. V. Naseh and S. Mosadegh, *World Acad. Sci. Eng. Technol.*, 2009, **25**, 159–162.
28. N. D. Hoa, N. Van Quy, L. Wei, M. An, H. Song, Y. Kang, Y. Cho and D. Kim, *J. Korean Phys. Soc.*, 2009, **54**, 1893.
29. Y. Jia, L. He, Z. Guo, X. Chen, F. Meng, T. Luo, M. Li and J. Liu, *J. Phys. Chem. C*, 2009, **113**, 9581–9587.
30. B. Ghaddab, F. Berger, J. B. Sanchez and C. Mavon, *Procedia Eng.*, 2010, **5**, 115–118.
31. R. Leghrib, R. Pavelko, A. Felten, A. Vasiliev, C. Cané, I. Gràcia, J.-J. Pireaux and E. Llobet, *Sensors Actuators B Chem.*, 2010, **145**, 411–416.
32. K.-Y. Choi, J.-S. Park, K.-B. Park, H. J. Kim, H.-D. Park and S.-D. Kim, *Sensors Actuators B Chem.*, 2010, **150**, 65–72.
33. C. Wongchoosuk, A. Wisitsoraat, A. Tuantranont and T. Kerdcharoen, *Sensors Actuators B Chem.*, 2010, **147**, 392–399.

34. R. Leghrib, A. Felten, J. J. Pireaux and E. Llobet, *Thin Solid Films*, 2011, **520**, 966–970.
35. S. Ahmadnia-Feyzabad, A. A. Khodadadi, M. Vesali-Naseh and Y. Mortazavi, *Sensors Actuators B Chem.*, 2012, **166-167**, 150–155.
36. A. Sharma, M. Tomar and V. Gupta, *J. Mater. Chem.*, 2012, **22**, 23608.
37. P. Tyagi, A. Sharma, M. Tomar, V. Gupta, *Sensors and Actuators, B: Chemical*, 2017, **248**, 980-986.
38. Y. Zhang, S. Cui, J. Chang, L. E. Ocola and J. Chen, *Nanotechnology*, 2013, **24**, 025503.
39. S. Mubeen, M. Lai, T. Zhang, J.-H. Lim, A. Mulchandani, M. A. Deshusses and N. V. Myung, *Electrochim. Acta*, 2013, **92**, 484–490.
40. V. M. Aroutiounian, A. Z. Adamyan, E. A. Khachaturyan, Z. N. Adamyan, K. Hernadi, Z. Pallai, Z. Nemeth, L. Forro, A. Magrez and E. Horvath, *Sensors Actuators B Chem.*, 2013, **177**, 308–315.
41. F. Mendoza, D. M. Hernández, V. Makarov, E. Febus, B. R. Weiner and G. Morell, *Sensors Actuators B Chem.*, 2014, **190**, 227–233.
42. C. Bittencourt, a. Felten, E. H. Espinosa, R. Ionescu, E. Llobet, X. Correig and J.-J. Pireaux, *Sensors Actuators B Chem.*, 2006, **115**, 33–41.
43. R. Ghasempour and a I. Zad, *J. Phys. D. Appl. Phys.*, 2009, **42**, 165105.
44. C. Wongchoosuk, A. Wisitsoraat, D. Phokharatkul, A. Tuantranont and T. Kerdcharoen, *Sensors (Basel)*, 2010, **10**, 7705–15.
45. P.-G. Su and T.-T. Pan, *Mater. Chem. Phys.*, 2011, **125**, 351–357.
46. M.-G. Willinger, G. Neri, A. Bonavita, G. Micali, E. Rauwel, T. Herntrich and N. Pinna, *Phys. Chem. Chem. Phys.*, 2009, **11**, 3615–22.
47. N. Du, H. Zhang, B. D. Chen, X. Y. Ma, Z. H. Liu, J. B. Wu and D. R. Yang, *Adv. Mater.*, 2007, **19**, 1641–1645.
48. W. Xuejing, L. Guanjun, Z. Fangkun and H. Linfeng, *J. chinese Ceram. Soc.*, 2012, **40**, 391–395.
49. J. Khanderi, R. C. Hoffmann, A. Gurlo and J. J. Schneider, *J. Mater. Chem.*, 2009, **19**, 5039.
50. D. Bai, Z. Zhang and K. Yu, *Appl. Surf. Sci.*, 2010, **256**, 2643–2648.

51. S. Palanisamy, S. Cheemalapati and S. Chen, *Int. J. Electrochem. Sci*, 2012, **7**, 8394–8407.
52. R. Vyas, S. Sharma, P. Gupta, A. K. Prasad, A. K. Tyagi, K. Sachdev and S. K. Sharma, *Adv. Mater. Res.*, 2012, **585**, 235–239.
53. M. Tak, V. Gupta and M. Tomar, *J. Mater. Chem. B*, 2013, **1**, 6392.
54. W. Li, H. Jung, N. D. Hoa, D. Kim, S.-K. Hong and H. Kim, *Sensors Actuators B Chem.*, 2010, **150**, 160–166.
55. G. Zhang, L. Dang, L. Li, R. Wang, H. Fu and K. Shi, *CrystEngComm*, 2013, **15**, 4730.
56. H. Heli and J. Pishahang, *Electrochim. Acta*, 2014, **123**, 518–526.
57. T. Ueda, K. Takahashi, F. Mitsugi and T. Ikegami, *Diam. Relat. Mater.*, 2009, **18**, 493–496.
58. M. Sánchez and M. E. Rincón, *Sensors Actuators, B Chem.*, 2009, **140**, 17–23.
59. S. Santangelo, G. Messina, G. Faggio, a. Donato, L. De Luca, N. Donato, a. Bonavita and G. Neri, *J. Solid State Chem.*, 2010, **183**, 2451–2455.
60. S. Mun, Y. Chen and J. Kim, *Sensors Actuators B Chem.*, 2012, **171-172**, 1186–1191.
61. M. Sánchez and M. E. Rincón, *Diam. Relat. Mater.*, 2012, **21**, 1–6.
62. M. B. Gholivand, M. Shamsipur and N. Amini, *Electrochim. Acta*, 2014, **123**, 569–575.
63. Z. Sun, H. Yuan, Z. Liu, B. Han and X. Zhang, *Adv. Mater.*, 2005, **17**, 2993–2997.
64. B. Sljukić, C. E. Banks and R. G. Compton, *Nano Lett.*, 2006, **6**, 1556–8.
65. R. Shanmugam, P. Barathi and A. S. Kumar, *Colloids Surfaces A Physicochem. Eng. Asp.*, 2014, **452**, 129–137.
66. N. Butwong, L. Zhou, W. Ng-eontae, R. Burakham, E. Moore, S. Srijaranai, J. H. T. Luong and J. D. Glennon, *J. Electroanal. Chem.*, 2014, **717-718**, 41–46.
67. J. Yang, L.-C. Jiang, W.-D. Zhang and S. Gunasekaran, *Talanta*, 2010, **82**, 25–33.
68. L.-C. Jiang and W.-D. Zhang, *Biosens. Bioelectron.*, 2010, **25**, 1402–7.
69. K. Zhang, N. Zhang, H. Cai and C. Wang, *Microchim. Acta*, 2012, **176**, 137–142.
70. Z. Yang, J. Feng, J. Qiao, Y. Yan, Q. Yu and K. Sun, *Anal. Methods*, 2012, **4**,

1924.

71. N. Quoc Dung, D. Patil, H. Jung and D. Kim, *Biosens. Bioelectron.*, 2013, **42**, 280–6.
72. H. Shekarchizadeh, M. Kadivar and A. A. Ensafi, *Chinese J. Catal.*, 2013, **34**, 1208–1215.
73. J. Chen, W.-D. Zhang and J.-S. Ye, *Electrochem. commun.*, 2008, **10**, 1268–1271.
74. B. Xu, M.-L. Ye, Y.-X. Yu and W.-D. Zhang, *Anal. Chim. Acta*, 2010, **674**, 20–6.
75. D. Jung, Y. Yoon and G. S. Lee, *Chem. Phys. Lett.*, 2013, **577**, 96–101.
76. G. An, Y. Zhang, Z. Liu, Z. Miao, B. Han, S. Miao and J. Li, *Nanotechnology*, 2008, **19**, 035504.
77. Z. Sun, X. Zhang, N. Na, Z. Liu, B. Han and G. An, *J. Phys. Chem. B*, 2006, **110**, 13410–4.
78. K. G. Ong and C. a. Grimes, *Sensors*, 2001, **1**, 193–205.
79. X. Zhou, H. Nie, Z. Yao, Y. Dong, Z. Yang and S. Huang, *Sensors Actuators B Chem.*, 2012, **168**, 1–7.
80. S. Dhall, and N. Jaggi, *Journal of Electronic Materials*, 2015, **45,** 695-702.
81. N. Q. Dung, D. Patil, H. Jung, J. Kim and D. Kim, *Sensors Actuators B Chem.*, 2013, **183**, 381–387.
82. B. Ghaddab, J. B. Sanchez, C. Mavon, M. Paillet, R. Parret, A. a. Zahab, J.-L. Bantignies, V. Flaud, E. Beche and F. Berger, *Sensors Actuators B Chem.*, 2012, **170**, 67–74.
83. Q. Huang, D. Zeng, H. Li and C. Xie, *Nanoscale*, 2012, **4**, 5651–8.
84. Y. X. Liang, Y. J. Chen and T. H. Wang, *Appl. Phys. Lett.*, 2004, **85**, 666.
85. Z. Zhang, R. Zou, G. Song, L. Yu, Z. Chen and J. Hu, *J. Mater. Chem.*, 2011, **21**, 17360.
86. G. Neri, S. G. Leonardi, M. Latino, N. Donato, S. Baek, D. E. Conte, P. a. Russo and N. Pinna, *Sensors Actuators B Chem.*, 2013, **179**, 61–68.
87. S. Mao, S. Cui, G. Lu, K. Yu, Z. Wen and J. Chen, *J. Mater. Chem.*, 2012, **22**, 11009.
88. J. S. Lee, O. S. Kwon, D. H. Shin and J. Jang, *J. Mater. Chem. A*, 2013, **1**, 9099.
89. C. Wongchoosuk, A. Wisitsoraat, D. Phokharatkul, M. Horprathum, A.

Tuantranont and T. Kerdcharoen, *Sensors Actuators B Chem.*, 2013, **181**, 388–394.

90. S. Srivastava, K. Jain, V. N. Singh, S. Singh, N. Vijayan, N. Dilawar, G. Gupta and T. D. Senguttuvan, *Nanotechnology*, 2012, **23**, 205501.
91. X. An, J. C. Yu, Y. Wang, Y. Hu, X. Yu and G. Zhang, *J. Mater. Chem.*, 2012, **22**, 8525.
92. S. Santangelo, G. Messina, G. Faggio, M.-G. Willinger, N. Pinna, A. Donato, A. Arena, N. Donato and G. Neri, *Diam. Relat. Mater.*, 2010, **19**, 590–594.
93. N. Chen, X. Li, X. Wang, J. Yu, J. Wang, Z. Tang and S. a. Akbar, *Sensors Actuators B Chem.*, 2013, **188**, 902–908.
94. S. Deng, V. Tjoa, H. M. Fan, H. R. Tan, D. C. Sayle, M. Olivo, S. Mhaisalkar, J. Wei and C. H. Sow, *J. Am. Chem. Soc.*, 2012, **134**, 4905–17.
95. L. T. Hoa, H. N. Tien, V. H. Luan, J. S. Chung and S. H. Hur, *Sensors Actuators B Chem.*, 2013, **185**, 701–705.
96. Y. Yang, C. Tian, L. Sun, R. Lü, W. Zhou, K. Shi, K. Kan, J. Wang and H. Fu, *J. Mater. Chem. A*, 2013, **1**, 12742.
97. S.-K. Lee, D. Chang and S. W. Kim, *J. Hazard. Mater.*, 2014, **268**, 110–4.
98. Q. Lin, Y. Li and M. Yang, *Sensors Actuators B Chem.*, 2012, **173**, 139–147.
99. M. Seredych and T. J. Bandosz, *Microporous Mesoporous Mater.*, 2012, **150**, 55–63.
100. J.-M. Tulliani, A. Cavalieri, S. Musso, E. Sardella and F. Geobaldo, *Sensors Actuators B Chem.*, 2011, **152**, 144–154.
101. P. Mbuyisa, S. P. Bhardwaj, F. Rigoni, E. Carlino, S. Pagliara, L. Sangaletti, A. Goldoni, M. Ndwandwe and C. Cepek, *Carbon N. Y.*, 2012, **50**, 5472–5480.
102. F. Rigoni, G. Drera, S. Pagliara, A. Goldoni, and L. Sangaletti, *Carbon*, 2014, **80**, 356-363.
103. K. R. Nemade and S. a. Waghuley, *Opt. Mater. (Amst).*, 2014, **36**, 712–716.
104. P. A. Russo, N. Donato, S. G. Leonardi, S. Baek, D. E. Conte, G. Neri and N. Pinna, *Angew. Chem. Int. Ed. Engl.*, 2012, **51**, 11053–7.
105. K. Anand, O. Singh, M. P. Singh, J. Kaur and R. C. Singh, *Sensors Actuators B Chem.*, 2014, **195**, 409–415.

106. Y. Chang, Y. Yao, B. Wang, H. Luo, T. Li and L. Zhi, *J. Mater. Sci. Technol.*, 2013, **29**, 157–160.
107. L. Zhou, F. Shen, X. Tian, D. Wang, T. Zhang and W. Chen, *Nanoscale*, 2013, **5**, 1564–9.
108. C. Karuppiah, S. Palanisamy, S.-M. Chen, V. Veeramani and P. Periakaruppan, *Sensors Actuators B Chem.*, 2014, **196**, 450–456.
109. F. Xu, M. Deng, G. Li, S. Chen and L. Wang, *Electrochim. Acta*, 2013, **88**, 59–65.
110. M. Liu, R. Liu and W. Chen, *Biosens. Bioelectron.*, 2013, **45**, 206–12.
111. X. Liu, H. Zhu and X. Yang, *Talanta*, 2011, **87**, 243–8.
112. Y. Ye, T. Kong, X. Yu, Y. Wu, K. Zhang and X. Wang, *Talanta*, 2012, **89**, 417–21.
113. L. Li, Z. Du, S. Liu, Q. Hao, Y. Wang, Q. Li and T. Wang, *Talanta*, 2010, **82**, 1637–41.
114. D. Ye, H. Li, G. Liang, J. Luo, X. Zhang, S. Zhang, H. Chen and J. Kong, *Electrochim. Acta*, 2013, **109**, 195–200.
115. P. Si, X.-C. Dong, P. Chen and D.-H. Kim, *J. Mater. Chem. B*, 2013, **1**, 110.
116. S. Palanisamy, S.-M. Chen and R. Sarawathi, *Sensors Actuators B Chem.*, 2012, **166-167**, 372–377.
117. S. K. Jha, C. N. Kumar, R. P. Raj, N. S. Jha and S. Mohan, *Electrochim. Acta*, 2014, **120**, 308–313.
118. P. Afzali, Y. Abdi and E. Arzi, *Sensors Actuators B Chem.*, 2014, **195**, 92–97.
119. J. Zhang, C. Zhao, P. A. Hu, Y. Q. Fu, Z. Wang, W. Cao, B. Yang and F. Placido, *RSC Adv.*, 2013, **3**, 22185.
120. X. Feng, J. Jiang, H. Ding, R. Ding, D. Luo, J. Zhu, Y. Feng and X. Huang, *Sensors Actuators B Chem.*, 2013, **183**, 526–534.
121. Z. Jiang, J. Wang, L. Meng, Y. Huang and L. Liu, *Chem. Commun.*, 2011, **47**, 6350–2.
122. S. Liang, J. Zhu, C. Wang, S. Yu, H. Bi, X. Liu and X. Wang, *Appl. Surf. Sci.*, 2014, **292**, 278–284.
123. H. Tian, H. Fan, H. Guo and N. Song, *Sensors Actuators B Chem.*, 2014, **195**,

132–139.

124. R. Zou, G. He, K. Xu, Q. Liu, Z. Zhang and J. Hu, *J. Mater. Chem. A*, 2013, **1**, 8445.
125. S.-J. Li, N. Xia, X.-L. Lv, M.-M. Zhao, B.-Q. Yuan and H. Pang, *Sensors Actuators B Chem.*, 2014, **190**, 809–817.
126. F. Yang, H. Su, Y. Zhu, J. Chen, W. M. Lau and D. Zhang, *Scr. Mater.*, 2013, **68**, 873–876.
127. F. Liu, X. Chu, Y. Dong, W. Zhang, W. Sun and L. Shen, *Sensors Actuators B Chem.*, 2013, **188**, 469–474.
128. D.-L. Zhou, J.-J. Feng, L.-Y. Cai, Q.-X. Fang, J.-R. Chen and A.-J. Wang, *Electrochim. Acta*, 2014, **115**, 103–108.
129. B. Yuan, C. Xu, L. Liu, Q. Zhang, S. Ji, L. Pi, D. Zhang and Q. Huo, *Electrochim. Acta*, 2013, **104**, 78–83.
130. H. Yu, M. Xu, S. Yu and G. Zhao, *Int. J. Electrochem. Sci.*,, 2013, **8**, 8050–8057.
131. C.-L. Sun, W.-L. Cheng, T.-K. Hsu, C.-W. Chang, J.-L. Chang and J.-M. Zen, *Electrochem. commun.*, 2013, **30**, 91–94.
132. Y.-W. Hsu, T.-K. Hsu, C.-L. Sun, Y.-T. Nien, N.-W. Pu and M.-D. Ger, *Electrochim. Acta*, 2012, **82**, 152–157.
133. L. Luo, L. Zhu and Z. Wang, *Bioelectrochemistry*, 2012, **88**, 156–63.
134. J. Song, L. Xu, C. Zhou, R. Xing, Q. Dai, D. Liu and H. Song, *ACS Appl. Mater. Interfaces*, 2013, **5**, 12928–34.
135. D. Ye, G. Liang, H. Li, J. Luo, S. Zhang, H. Chen and J. Kong, *Talanta*, 2013, **116**, 223–30.
136. J. Zhang, X. Zhu, H. Dong, X. Zhang, W. Wang and Z. Chen, *Electrochim. Acta*, 2013, **105**, 433–438.
137. Y. Zhang, Y. Wang, J. Jia and J. Wang, *Sensors Actuators B Chem.*, 2012, **171-172**, 580–587.
138. B. Yuan, C. Xu, D. Deng, Y. Xing, L. Liu, H. Pang and D. Zhang, *Electrochim. Acta*, 2013, **88**, 708–712.
139. W. Lv, F.-M. Jin, Q. Guo, Q.-H. Yang and F. Kang, *Electrochim. Acta*, 2012, **73**, 129–135.

140. X. Li, A. Hu, J. Jiang, R. Ding, J. Liu and X. Huang, *J. Solid State Chem.*, 2011, **184**, 2738–2743.
141. R. S. Dey and C. R. Raj, *RSC Adv.*, 2013, **3**, 25858.
142. T. Kavitha, A. I. Gopalan, K.-P. Lee and S.-Y. Park, *Carbon,* 2012, **50**, 2994–3000.
143. Z. Luo, X. Ma, D. Yang, L. Yuwen, X. Zhu, L. Weng and L. Wang, *Carbon*, 2013, **57**, 470–476.
144. C. Marichy, P. A. Russo, M. Latino, J.-P. Tessonnier, M.-G. Willinger, N. Donato, G. Neri, and N. Pinna, *J. Phys. Chem. C*, 2013, **117**, 19729−19739
145. C. Marichy, N. Donato, M.-G. Willinger, M. Latino, D. Karpinsky, S.-H. Yu, G. Neri, and N. Pinna, *Adv. Funct. Mater*. 2011, **21**, 658−666.
146. E. Llobet, R. Ionescu, E. H. Espinoza, R. Leghrib, A. Felten, and R. Erni, *Sensors and Actuators B: Chemical*, 2008, **131**, 174
147 J. Liu, X. Wang, Q. Peng, and Y. Li , *Sensors and Actuators, B: Chemical*, 2006 **115**, 481-487
148 Hyung-Sik Woo, ChanWoong Na, Il-Doo Kim and Jong-Heun Lee, , *Nanotechnology*, 2012, **23,** 245501
149 G. Lu, L. E. Ocola, and J. Chen, *Adv. Mater*. 2009, **21**, 2487–2491
150. D. Jung, J. Kim, and G. S. Lee, *Sensors and Actuators A* 2015, **223**, 11–17
151. Wei.De Zhang, Bin Xu, and Liao-Chuan Jiang, *Jour. of Materials Chemistry*, 2010, **20**, 6383-6391
152. T. Ueda, K. Takahashi, F. Mitsugi, T. Ikegami, Diamond and Related Materials, 2009, **18**, 493-496
153. F. Rigoni, G. Drera, S. Pagliara, E. Perghem, C. Pintossi, A. Goldoni, L. Sangaletti, *Nanotechnology*, 2016, **28**, 03550
154. A. Zahab, L. Spina, P. Poncharal, C. Marlière, *Phys. Rev. B*, 2000, **62**, 10000-10003
155. D.R. Kauffman, A. Star, *small*, 2007, **3**, 1324 – 1329
156. S.Gupta Chatterjee, S. Chatterjee, A.K. Ray, and A.K. Chakraborty, (2015) *Sensors and Actuators, B: Chemical*, 2015, **221**, 1170-1181
157. J. T. Robinson, F. K. Perkins, E. S. Snow, Z. Wei and P. E. Sheehan, *Nano Lett.*,

2008, **8**, 3137–40.

158. H. Zhang, J. Feng, T. Fei, S. Liu and T. Zhang, *Sensors Actuators B Chem.*, 2014, **190**, 472–478.